

Efficient perturbation theory to improve the density matrix renormalization group

Emanuele Tirrito,¹ Shi-Ju Ran,¹ Andrew J. Ferris,¹ Ian P. McCulloch,² and Maciej Lewenstein^{1,3,*}

¹*ICFO—Institut de Ciències Fòniques, The Barcelona Institute of Science and Technology, 08860 Castelldefels (Barcelona), Spain*

²*Centre for Engineered Quantum Systems, School of Physical Sciences, The University of Queensland, Brisbane, Queensland 4072, Australia*

³*ICREA—Institució Catalana de Recerca i Estudis Avançats, Lluís Companys 23, 08010 Barcelona, Spain*

(Received 25 August 2016; revised manuscript received 21 January 2017; published 21 February 2017)

The density matrix renormalization group (DMRG) is one of the most powerful numerical methods available for many-body systems. It has been applied to solve many physical problems, including the calculation of ground states and dynamical properties. In this work, we develop a perturbation theory of the DMRG (PT-DMRG) to greatly increase its accuracy in an extremely simple and efficient way. Using the canonical matrix product state (MPS) representation for the ground state of the considered system, a set of orthogonal basis functions $\{|\psi_i\rangle\}$ is introduced to describe the perturbations to the ground state obtained by the conventional DMRG. The Schmidt numbers of the MPS that are beyond the bond dimension cutoff are used to define these perturbation terms. The perturbed Hamiltonian is then defined as $\tilde{H}_{ij} = \langle\psi_i|\hat{H}|\psi_j\rangle$; its ground state permits us to calculate physical observables with a considerably improved accuracy compared to the original DMRG results. We benchmark the second-order perturbation theory with the help of a one-dimensional Ising chain in a transverse field and the Heisenberg chain, where the precision of the DMRG is shown to be improved $O(10)$ times. Furthermore, for moderate L the errors of the DMRG and PT-DMRG both scale linearly with L^{-1} (with L being the length of the chain). The linear relation between the dimension cutoff of the DMRG and that of the PT-DMRG at the same precision shows a considerable improvement in efficiency, especially for large dimension cutoffs. In the thermodynamic limit we show that the errors of the PT-DMRG scale with $\sqrt{L^{-1}}$. Our work suggests an effective way to define the tangent space of the ground-state MPS, which may shed light on the properties beyond the ground state. This second-order PT-DMRG can be readily generalized to higher orders, as well as applied to models in higher dimensions.

DOI: [10.1103/PhysRevB.95.064110](https://doi.org/10.1103/PhysRevB.95.064110)

I. INTRODUCTION

In the last three decades, strongly correlated quantum many-body systems have remained at the center of scientific interest and define the most important challenges and open questions [1–4]. For instance, understanding certain classes of quantum many-body systems is necessary for understanding the mechanism of high- T_c superconductivity (cf. [5,6]) or topological phase transitions (cf. [7,8]) and spin liquids (cf. [9]; for a recent experiment see [10]). These systems are notoriously hard to study analytically or numerically. Exact solutions are extremely rare for these kinds of systems. In fact, the Bethe ansatz works well only for one-dimensional systems (cf. [11–13]). In various mean-field theories, the role of quantum fluctuations is usually underestimated. For these reasons, novel efficient numerical approaches are greatly desired. These new approaches naturally encounter great challenges, because the dimension of the Hilbert space of considered systems increases exponentially with the number of particles. This limits significantly the applicability not only of exact diagonalization methods [14], but even of quantum Monte Carlo methods [15]; the latter can be applied to larger systems, but they face the fatal negative-sign problem for fermionic and frustrated systems.

One of the most important numeric tools developed in the last decades is the method based on tensor networks (TNs) [16,17]. It offers an efficient representation of quantum

many-body states that coincides with their entanglement structure. It takes advantage of the fact that not all quantum states in the Hilbert space of many-body systems with (in particular, short-range) interactions are equally relevant for low-energy and low-temperature physics. It has been found, namely, that the low-lying eigenstates of gapped Hamiltonians with local interactions obey the so-called area law of entanglement entropy [18–25]. Specifically speaking, for a spatial subregion \mathcal{R} of the physical space where the system is defined, the reduced density matrix is defined as $\hat{\rho}_{\mathcal{R}} = \text{Tr}_{\mathcal{E}}(\hat{\rho})$, with \mathcal{E} denoting the spatial complement of the subregion \mathcal{R} . The entanglement entropy is defined as

$$S(\hat{\rho}_{\mathcal{R}}) = -\text{Tr}\{\hat{\rho}_{\mathcal{R}}\log(\hat{\rho}_{\mathcal{R}})\}. \quad (1)$$

Then the area law of entanglement entropy reads

$$S(\hat{\rho}_{\mathcal{R}}) = O(|\partial\mathcal{R}|), \quad (2)$$

with $|\partial\mathcal{R}|$ the length of the boundary. In particular, for a D -dimensional lattice, one has

$$S = O(L^{D-1}), \quad (3)$$

with L being the length scale. This means that for one-dimensional (1D) systems, $S = \text{const}$. The area law suggests that low-lying eigenstates stay in a “small corner” of the full Hilbert space of the many-body system and that they can be described by a much smaller number of parameters. This subset of states can be well approximated by TN states.

The density matrix renormalization group (DMRG) [26,27] is one of the most famous tensor network methods, based on the so-called matrix product state (MPS), a 1D TN-state

*maciej.lewenstein@icfo.es

ansatz [16]. The DMRG algorithm was formulated by S. White in 1992 for calculating ground-state properties of strongly correlated 1D systems [28,29]. The original DMRG is a variant of Wilson’s numeric renormalization group [30] with Hilbert space decimations and reduced basis transformations. Instead of truncating the eigenstates of the Hamiltonian according to their energies, the selection is based on their weights in the reduced density matrices, i.e., the entanglement. Such a strategy improves the performance largely. It was then realized by Östlund and Rammer that the block states in the DMRG can be represented as the MPS [31]; they predicted the properties of the entanglement spectrum, such as the area law [22,23]. Verstraete *et al.* reinterpreted the DMRG algorithm as a variational principle from the perspective of quantum information theory [32].

The DMRG has extremely wide applications in strongly correlated 1D systems, e.g., for simulating ground-state properties of 1D spin [33] or Hubbard [3,34–38] chains. Referring to the spin models, the DMRG accurately gives the excitation gap of the $S = 1$ Heisenberg chain [39] or the Haldane gap [40,41]. The DMRG also shows great efficiency when applied to fermionic systems, such as the 1D Hubbard model and t - J model [42], where logarithmic corrections to the correlations were found, compared with the $S = 1/2$ Heisenberg chain. Moreover, the DMRG has been used to study the topological order and quantum Hall effect [43,44].

The DMRG has also been extended to two-dimensional (2D) models [45], and one of the most remarkable achievements of the DMRG is the demonstration of the quantum spin-liquid behavior in frustrated 2D magnets that break no symmetries even down to zero temperature [9]. By calculating the topological entanglement entropy [46], strong evidence of a spin-liquid ground state was found using the DMRG for a Heisenberg antiferromagnet on a kagome lattice [47]. The DMRG has also been used to identify spin-liquid phases stabilized by anisotropic next-to-next-neighbor and multispin interactions [48–52]. But the 2D DMRG suffers from finite-size effects, and thus definitive evidence of the existence of isotropic spin models with short-range interactions [53–56], whose ground states break no symmetries, is still missing.

The DMRG method was also developed for the study of dynamic properties, such as dynamical structure functions and frequency-dependent conductivities [57–60]. At the same time, its finite-temperature extensions to 2D classical [61] and 1D quantum [62,63] systems demonstrate a good performance and precision. It has even been utilized for the more demanding study of non-Hermitian (pseudo-) Hamiltonians emerging in the analysis of relaxation towards classical steady states in 1D systems far from equilibrium [64–66].

In this paper we develop a perturbation theory of the DMRG (PT-DMRG) that provides a remarkably efficient way to improve the precision of the DMRG and defines a tangent space [67] of the ground state, which is important for extracting the information about the model. We define a set of states forming an orthogonal basis $\{|\psi_i\rangle\}$, obtained from the conventional DMRG. The perturbed Hamiltonian is then defined as $\tilde{H}_{ij} = \langle\psi_i|\hat{H}|\psi_j\rangle$. The ground state of \tilde{H} permits us to calculate physical observables with a considerably improved accuracy compared to the original DMRG results. The improvement in accuracy is due to the fact that the

PT-DMRG captures the ground state not only with one MPS but with a superposition of multiple orthogonal MPSs. This means that we can codify more entanglement. We test our method on the quantum Ising model in a transverse field and on the Heisenberg model. In particular, we show how the error committed by the DMRG and PT-DMRG scales with the bond dimension χ and the length of the chain L . Without increasing the computation costs much, the error is reduced by about $O(10)$ times using the PT-DMRG. Other perturbation schemes are explained in [68–70].

We would like to stress that the MPS represents states in a subspace of the complete Hilbert space. The area law suggests that low-lying eigenstates stay in a “small corner” of the full Hilbert space of the many-body system and that they can be described by a much smaller number of parameters. This subset of states can be well approximated by TN states. In general, for 1D systems the MPS is an optimal representation of all the states that verify the area law. In this tiny corner the ground states of local Hamiltonians live. Our claim is not to find another representation of the ground state, but to find a better approximation of the ground state than the standard DMRG, by extending the variational ansatz to superpositions. This does not mean that the MPS is suboptimal for the ground state, but that the MPS found through a DMRG is approximated. In fact the DMRG gives us the best approximated MPS that represents a ground state, and not an exact ground state. The error that we obtain is because we neglect the second largest singular values that contribute to the entropy [see Eq. (10)]. To recover this information we propose a new method. We define a new basis in which we codify the entanglement, which was lost in the normal DMRG. Using a superposition of the MPS we define a new ansatz. Therefore, the ground state obtained with the PT-DMRG captures more entanglement than the MPS with the standard DMRG. This is the essential reason for the better precision of our method. In other words, it gives a better approximation of the ground state of strongly correlated many-body systems by recovering the leading term of entanglement, which is discarded in the standard truncations of the DMRG.

This paper is organized as follows: In Sec. II, we briefly review the DMRG and present some discussion of its convergence properties. In Secs. III and IV, we describe the PT-DMRG and discuss its properties. In Sec. V, we discuss the numerical results on the quantum transverse Ising model. In Sec. V a summary and an outlook are presented.

II. DENSITY MATRIX RENORMALIZATION GROUP

Let us consider a 1D quantum system consisting of L sites. Each lattice site has physical degrees of freedom denoted $|\sigma_j\rangle$ in a local d -dimensional Hilbert space $\mathcal{H}_d = \mathcal{C}^d$. A pure state can be generally written in a local basis as

$$|\psi\rangle = \sum_{\sigma_1 \dots \sigma_L} C_{\sigma_1 \dots \sigma_L} |\sigma_1 \dots \sigma_L\rangle, \quad (4)$$

with $C_{\sigma_1 \dots \sigma_N}$ coefficients of the state. If the lattice has open boundary conditions, $C_{\sigma_1 \dots \sigma_N}$ can be rewritten in an MPS using a series of singular value decomposition (SVD) as

$$|\psi\rangle = \sum_{\sigma_1 \dots \sigma_L} M_{1,a_1}^{\sigma_1} M_{a_1,a_2}^{\sigma_2} \dots M_{a_{L-1},1}^{\sigma_L} |\sigma_1 \dots \sigma_L\rangle, \quad (5)$$

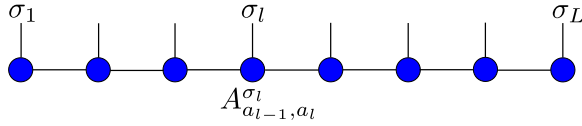


FIG. 1. Graphical representation of the matrix product state (MPS).

where $M_{a_{i-1}, a_i}^{\sigma_i}$ is a third-order tensor, i.e., a $(\chi_{i-1} \times \chi_i)$ matrix for each value of σ_i , with χ_i the bond dimension of the index a_i (Fig. 1). The state represented in Eq. (5) is called the matrix product state. Instead of M^{σ_i} , we also write A^{σ_i} (B^{σ_i}) for a left (right) normalized MPS tensor:

$$\sum_{\sigma_i} A^{\sigma_i \dagger} A^{\sigma_i} = I, \quad \sum_{\sigma_i} B^{\sigma_i} B^{\sigma_i \dagger} = I. \quad (6)$$

Similarly, a Hamiltonian operator can be written as a matrix product operator (MPO) [71–73], i.e.,

$$\hat{H} = \hat{W}_{1, b_1}^{[1]} \hat{W}_{b_1, b_2}^{[2]} \cdots \hat{W}_{b_{L-1}, 1}^{[L]}, \quad (7)$$

where $\hat{W}^{[l]} = \sum_{\sigma_i, \sigma'_i} W^{\sigma_i \sigma'_i} |\sigma_i\rangle \langle \sigma'_i|$ is defined in a local Hilbert space (Fig. 2) and χ_W is the bond dimension of the index b_i .

In order to find the ground state of a many-body system one solves a standard variational problem using the matrix elements of the MPS as variational parameters. Ideally, the minimization should be done simultaneously over all the coefficients of all tensors. However, this is quite difficult and inefficient to implement. Following the original procedure [28,29], the strategy of the DMRG that we use here is to minimize two tensors each time while keeping the others fixed. Then we move to another pair of tensors and repeat the procedure until convergence.

Furthermore, we define $L_0 = 1$ and $L_i = L_{i-1} A_i^\dagger W_i A_i$ with summation over all possible indices. Similarly, the right environment $R_{L+1} = 1$ is defined by $R_i = B_i^\dagger W_i B_i R_{i+1}$. With these contractions it is possible to write

$$\langle \psi | \hat{H} | \psi \rangle = L_{i-1} D_{i, i+1}^\dagger W_i W_{i+1} D_{i, i+1} R_{i+2} \quad (8)$$

for any $i \in [0, L]$, where $D^{\sigma_i, \sigma_{i+1}} = \sum M^{\sigma_i} M^{\sigma_{i+1}}$. Therefore the optimization of the variational parameters of the MPS is implemented as a local update step. The local update step amounts to the solution of a generalized eigenvalue problem,

$$H_{\text{eff}} D - \lambda D = 0, \quad (9)$$

where $H_{\text{eff}} = L_{i-1} W_i W_{i+1} R_{i+1}$ is the effective Hamiltonian. (The technical details are explained in the Appendix.) The updated MPS is obtained from the sSVD of the generalized

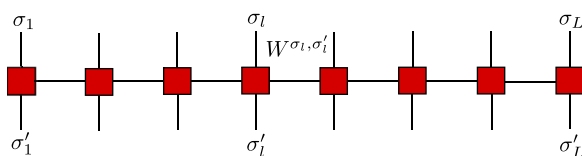


FIG. 2. Matrix product operator representation of \hat{H} . At each site a four-rank tensor $\hat{W}_{a_{i-1}, a_i}^{\sigma_i \sigma'_i}$ is defined.

eigenvector D :

$$D_{\alpha\beta}^{\sigma_i \sigma_{i+1}} = \sum_{\rho} U_{\sigma_i \alpha, \rho} S_{\rho} V_{\rho, \sigma_{i+1} \beta}. \quad (10)$$

Take only the χ largest singular vectors in U as the new tensor $A_{a_{i-1}, \rho}^{\sigma_i}$, i.e., $A_{a_{i-1}, \rho}^{\sigma_i} = U_{\sigma_i a_{i-1}, \rho}$ when sweeping from left to right, and take the χ largest singular vectors in V as the new tensor $A_{\rho, a_{i+1}}^{\sigma_{i+1}}$ when sweeping from right to left. In this way, the left and right orthogonal conditions of the MPS are automatically fulfilled.

Specifically speaking, a left-to-right (or right-to-left) sweep consists of the following steps:

(i) Start with a random initial MPS and transform it in the right orthogonal form or, alternatively, start from a ground state found with the iDMRG.

(ii) Optimize the tensor $D^{\sigma_i \sigma_{i+1}}$: construct the environment L and R and solve the standard eigenvalue problem, (9).

(iii) Carry out an SVD of $D^{\sigma_i \sigma_{i+1}}$ and update the tensor A^{σ_i} .

(iv) Repeat the same operations for every site until reaching the preset convergence:

$$\langle \psi | \hat{H}^2 | \psi \rangle - (\langle \psi | \hat{H} | \psi \rangle)^2 \rightarrow 0. \quad (11)$$

To analyze the computational cost we have to take special care to ensure optimal ordering of multiplications when dealing with each eigensolver given by (9). The problem is to contract $L_{i-1} W_i W_{i+1} R_{i+2} D^{\sigma_i \sigma_{i+1}}$, with $L_{i-1} R_{i+2} \in (\chi, \chi_W, \chi)$, $W_i \in (d, \chi_W, d \chi_W)$, and $D^{\sigma_i \sigma_{i+1}} \in (\chi, d, \chi)$. The optimal ordering should be $((L_{i-1} D^{\sigma_i \sigma_{i+1}}) W_i W_{i+1}) R_{i+1}$, and in the way, one has to

(a) Contract L_{i-1} and $D^{\sigma_i \sigma_{i+1}}$ over the left MPS bond at a cost $O(\chi^3 \cdot \chi_W \cdot d^2)$.

(b) Multiply by $W_i W_{i+1}$ over the physical bond of $D^{\sigma_i \sigma_{i+1}}$ at a cost $O(\chi^2 \cdot \chi_W^2 \cdot d^4)$.

(c) Contract with R_{i+2} over the right MPO and MPS bond at a cost $O(\chi^3 \cdot d^2 \cdot \chi_W)$.

The total cost of this procedure to apply \hat{H} to $|\psi\rangle$ is $O(\chi^3 \cdot \chi_W \cdot d^2 + \chi^2 \cdot \chi_W^2 \cdot d^4 + \chi^3 \cdot d^2 \cdot \chi_W)$.

III. SUBSPACE EXPANSION

In the following, we develop a second-order perturbation theory for the DMRG. Note that from the orthogonality the contribution of the first-order term is 0. This optimization permits the recovery of some of the lost information, due to the truncation in the SVD of $D^{\sigma_i \sigma_{i+1}}$, and reaching a better approximation of the ground state. In the last section, we have shown how the DMRG works and where its error comes from. To reduce the error, we define a new orthogonal basis $\{|\psi_i\rangle\}$, whose elements have the MPS form. We put an impurity bond in each $\{|\psi_i\rangle\}$ so that it is orthogonal to the ground state obtained by the DMRG. To define this impurity bond [e.g., between the i th and the $(i+1)$ th sites], we consider the SVD of $D^{\sigma_i \sigma_{i+1}}$ and the tensor \tilde{A}^{σ_i} as the second χ largest singular vectors. Thus, \tilde{A}^{σ_i} is orthogonal to the tensor A^{σ_i} in the original MPS.

By introducing one impurity in different bonds of $|\psi_0\rangle$, we can define a new basis $\{|\psi_i\rangle\}$. Since both are in orthogonal

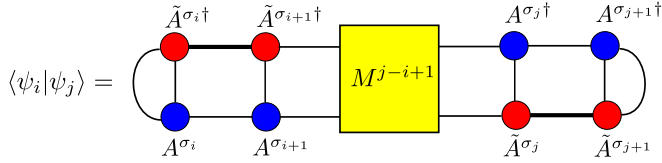


FIG. 3. Graphical representation of the overlap $\langle \psi_i | \psi_j \rangle$ represented in Eq. (12).

form, one has

$$\begin{aligned} \langle \psi_i | \psi_j \rangle = & \sum_{a_{i+1} a'_{i+1} a_{j-1} a'_{j-1}} A_{a_{i-1}, a_i}^{\sigma_i} \tilde{A}_{a_{i-1}, a'_i}^{\sigma_i \dagger} A_{a_i, a_{i+1}}^{\sigma_{i+1}} \tilde{A}_{a'_i, a'_{i+1}}^{\sigma_{i+1} \dagger} \\ & \times M_{a_{i+1} a'_{i+1}, a_{j-1} a'_{j-1}}^{j-i+1} \tilde{A}_{a_{j-1}, a_j}^{\sigma_j} A_{a'_{j-1}, a'_j}^{\sigma_j \dagger} \tilde{A}_{a_j, a_{j+1}}^{\sigma_{j+1}} A_{a'_j, a'_{j+1}}^{\sigma_{j+1} \dagger}, \end{aligned} \quad (12)$$

where M is the transfer matrix of the overlap $\langle \psi_i | \psi_j \rangle$ (see Fig. 3). Thus, $|\psi_i\rangle$ and $|\psi_j\rangle$ are orthogonal to each other for $i \neq j$.

Now one can define the perturbed Hamiltonian $\hat{\mathcal{H}}$ with $\{|\psi_i\rangle\}$ ($i = 0, 1, \dots$). Note that $|\psi_0\rangle$ is the ground state with the original DMRG. The matrix elements of $\hat{\mathcal{H}}$ are defined as

$$\mathcal{H}_{ij} = \langle \psi_i | \hat{\mathcal{H}} | \psi_j \rangle \quad (13)$$

and form the matrix \mathcal{H} . The ground-state energy is calculated as

$$\tilde{E}_0 = \frac{\langle \tilde{\psi}_0 | \hat{\mathcal{H}} | \tilde{\psi}_0 \rangle}{\langle \tilde{\psi}_0 | \tilde{\psi}_0 \rangle}, \quad (14)$$

where $|\tilde{\psi}_0\rangle$ is defined as the combination of $\{|\psi_i\rangle\}$,

$$|\tilde{\psi}_0\rangle = \sum_j \Psi_j |\psi_j\rangle, \quad (15)$$

where Ψ_j are the coordinates of the dominant eigenvector of $\hat{\mathcal{H}}$. By using the basis $\{|\psi_i\rangle\}$, the perturbed ground-state energy is simply obtained as

$$\tilde{E}_0 = \sum_{ij} \Psi_j^\dagger \mathcal{H}_{ij} \Psi_j. \quad (16)$$

IV. PERTURBATION THEORY DMRG

Now we explain how to implement the PT-DMRG in practice. Using the notation introduced above, the steps mostly follow the standard DMRG. In the outermost loop, the update sweeps over the system from left to right and right to left until the preset convergence is reached. The inner loop sweeps over the system, iterating over and updating the tensors at each site sequentially. Each local update during a left-to-right sweep consists of the following steps:

(i) Perform the standard DMRG to obtain the ground state MPS $|\psi_0\rangle$ (which is assumed in the right-orthogonal form).

(ii) From left to right, calculate $D^{\sigma_i \sigma_{i+1}}$ and perform an SVD for each i ; keep the second χ largest left and right singular vectors as \tilde{A}^{σ_i} and $\tilde{A}^{\sigma_{i+1}}$, respectively.

(iii) Construct the orthogonal basis $\{|\psi_i\rangle\}$ by introducing an impurity \tilde{A}^{σ_i} in different bonds.

(iv) Construct the perturbed Hamiltonian $\hat{\mathcal{H}}$ according to Eq. (13) and calculate its dominant eigenvector Ψ .

(v) Calculate the perturbed ground state of the system as

$$|\tilde{\psi}_0\rangle = \sum_{i=1}^N \Psi_i |\psi_i\rangle. \quad (17)$$

As regards the computational cost, the additional cost compared with the DMRG arises from the construction of \mathcal{H} defined in Eq. (13) and its diagonalization. The cost of $\langle \psi_i | \hat{H} | \psi_j \rangle$ is $O(\chi^3 d \chi_w)$, therefore the construction of \mathcal{H} costs $O(N \chi^3 d \chi_w)$, where N is the number of elements of the perturbed basis. The diagonalization of \mathcal{H} costs $O(N^3)$. Therefore the full cost for the perturbation theory is $O(N \chi^3 d \chi_w) + O(\chi^2) + O(N^3)$. Note that the diagonal and first row/column of \mathcal{H} can be obtained easily during the final DMRG sweep itself, which makes it much computationally cheaper. The additional computational memory one needs to store the perturbations equals $O(d^2 \chi^2 N) + O(N)$.

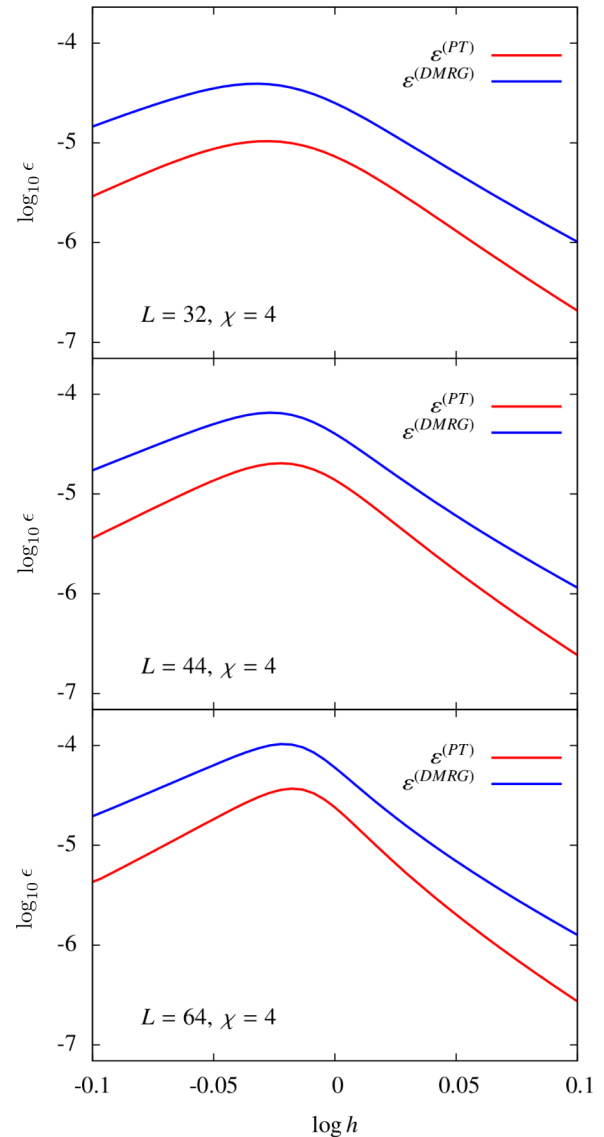


FIG. 4. Error ϵ of the 1D Ising model on a 32,44,64 chain with open boundary conditions as a function of h . The error of the PT-DMRG method with bond dimension $\chi = 4$ is more than $O(10)$ times smaller compared with the error of the standard DMRG.

V. NUMERICAL RESULTS

A. Quantum transverse Ising model

To illustrate our method we study the 1D spin-half quantum Ising model in a transverse field, especially near the quantum phase transition. The Hamiltonian reads

$$\hat{H} = -J \sum_{i=1}^L \hat{\sigma}_i^x \hat{\sigma}_{i+1}^x + h \sum_{i=1}^L \hat{\sigma}_i^z. \quad (18)$$

In the infinite case, a quantum phase transition occurs at $h/J = 1$. The system for $h/J > 1.0$ is in a paramagnetic phase with an order parameter $\langle S^z \rangle \neq 0$ and in a ferromagnetic phase for $h/J < 1.0$ with an order parameter $\langle S^x \rangle \neq 0$. At the critical point, both order parameters go to 0. We set $J = 1$ as the energy scale.

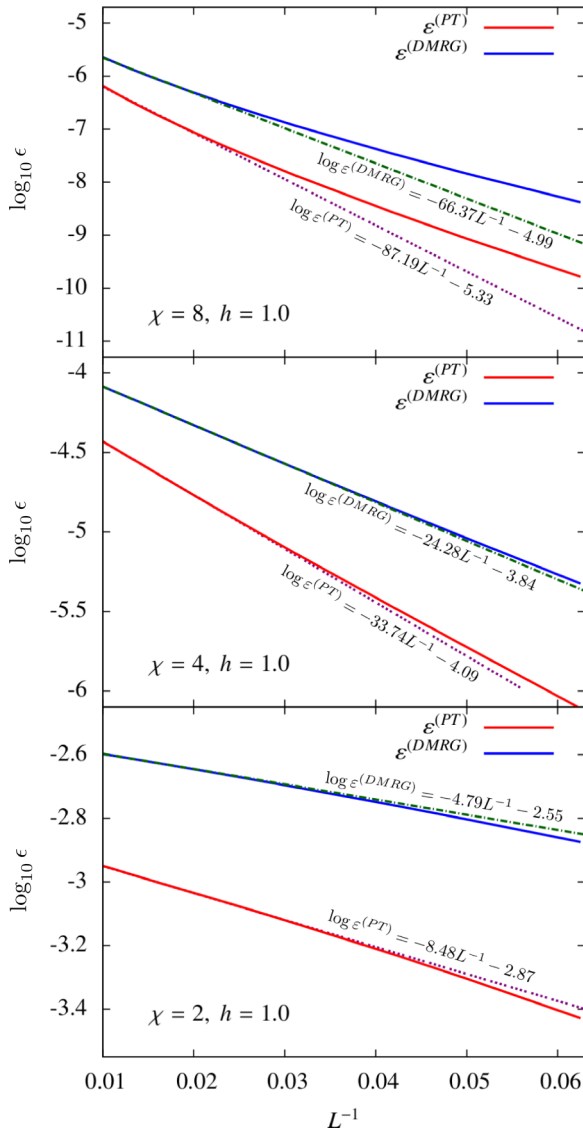


FIG. 5. Error ε of the 1D Ising model as a function of the length in the quantum phase transition $h = 1.0$, for different values of χ : 2, 4, and 8. We show that the error for the PT-DMRG is much smaller. The PT-DMRG gives a systematic improvement in accuracy.

In the numerical simulations, we considered a finite-size system with open boundary conditions with the length $L = 16$ –128. To benchmark the PT-DMRG, we compute the ground-state energies of the DMRG and PT-DMRG with the same bond dimension χ and compare them with the (quasiexact) results from the DMRG with sufficiently large χ , i.e., $\chi = 100$ –400 (note that χ for quasiexact calculations changes according to the length of the chain, in other words, the entanglement). The error is defined as

$$\varepsilon = \frac{E_0 - \langle \psi | \hat{H} | \psi \rangle}{E_0}, \quad (19)$$

with E_0 the energy from the quasiexact DMRG.

Figure 4 shows the error with $L = 32, 44$, and 64 versus the magnetic field h . We compare the results of the conventional DMRG and PT-DMRG for $\chi = 2, 4$, and 8 . Near the phase transition, the error of the PT-DMRG is more than $O(10)$ times smaller compared with the error of the conventional DMRG with the same χ . Our simulations suggest that through the PT-DMRG, we are able to retrieve the leading term of the lost information with the truncations in the SVD. Therefore, the ground state with the PT-DMRG captures more entanglement than the MPS with the standard DMRG, which is the essential reason for the better precision of our method, especially near the critical point.

In Fig. 5, we show the error against L^{-1} for $h = 1$ (critical point). The results show that the error increases linearly with L^{-1} for both the DMRG and the PT-DMRG, indicating a systematic improvement in the accuracy for moderate values of L . For the thermodynamic limit the error of the PT-DMRG scales as $\sqrt{L^{-1}}$, for reasons explained below.

In Fig. 6, we show the error against χ for $h = 1$ (phase transition) and for $L = 64$. The results show that the error decreases with the bond dimension χ for the DMRG and PT-DMRG. The error of the PT-DMRG decreases more rapidly than that of the standard DMRG. This shows a considerable improvement in the accuracy for any value of the bond dimension χ near the phase transition. This is due to the fact

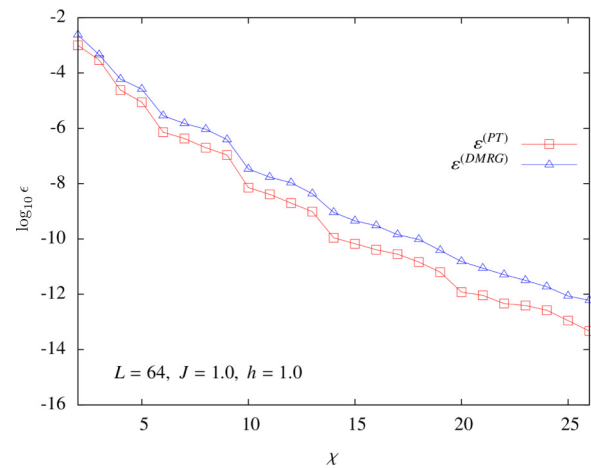


FIG. 6. Error ε of the 1D Ising model versus χ in the quantum phase transition $h = 1.0$ for $L = 64$. We show how the error of the PT-DMRG decreases more rapidly than the error of the standard DMRG.

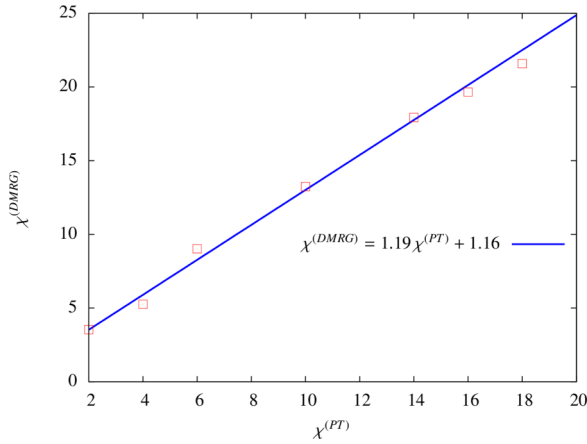


FIG. 7. The plot is the fit between $\chi^{(DMRG)}$ and $\chi^{(PT)}$ of the 1D Ising model in the quantum phase transition $h = 1.0$ for $L = 64$. We show how the PT-DMRG requires a smaller bond dimension χ than the DMRG.

that the PT-DMRG uses a new ansatz to capture the ground state.

To see more clearly the improvement in the efficiency of the PT-DMRG, we study the correspondence between the bond dimension cutoff $\chi^{(DMRG)}$ of the standard DMRG and that of the PT-DMRG $\chi^{(PT)}$. As shown in Fig. 7, each pair of $\chi^{(DMRG)}$ and $\chi^{(PT)}$ given by the data points has approximately the same precision. In detail, to determine $\chi^{(DMRG)}$ for a given $\chi^{(PT)}$, we first find two χ 's with the DMRG, where the precision of one χ is higher than the precision of the PT-DMRG with $\chi^{(PT)}$, and the other is lower. Then we do a fit to find $\chi^{(DMRG)}$, which is a fraction between these two χ 's.

We choose $h = 1$ and $L = 64$. The results show that with each $\chi^{(PT)}$ in the PT-DMRG, we need a larger bond dimension cutoff (i.e., to keep more states) in the DMRG to reach the same precision. We also find a linear relation between $\chi^{(PT)}$ and $\chi^{(DMRG)}$:

$$\chi^{(DMRG)} = 1.19\chi^{(PT)} + 1.16. \quad (20)$$

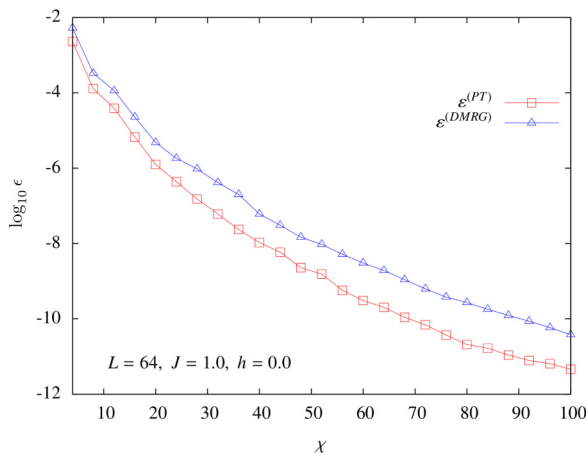


FIG. 8. Error ϵ of the 1D Heisenberg model versus χ for $h = 0.0$ and $L = 64$. We show how the error of the PT-DMRG decrease more rapidly than the error of the standard DMRG.

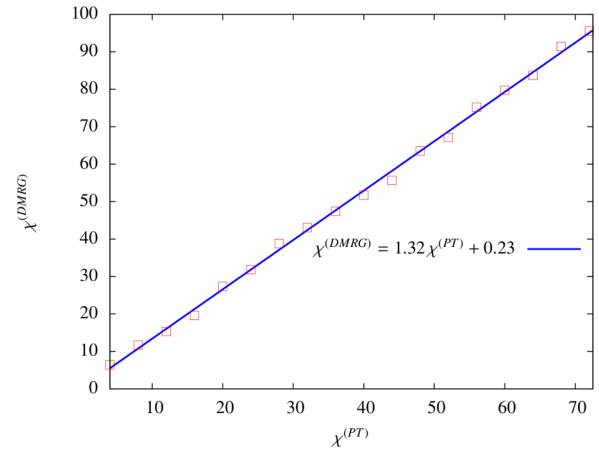


FIG. 9. The plot is the fit between $\chi^{(DMRG)}$ and $\chi^{(PT)}$ of the 1D Heisenberg model in the quantum phase transition $h = 0.0$ for $L = 64$. We show how the PT-DMRG requires a smaller bond dimension χ than the DMRG.

Since the computational cost an MPS takes scales as $\sim \chi^2$ (2 is the number of the virtual bond in each local tensor of the MPS), such a linear relation suggests that the larger the χ one uses, the more computational resources one can save by using the PT-DMRG.

B. Heisenberg model

We study also the 1D spin-1/2 quantum Heisenberg model, where the Hamiltonian reads

$$\hat{H} = -J \sum_{i=1}^L (\hat{\sigma}_i^x \hat{\sigma}_{i+1}^x + \hat{\sigma}_i^y \hat{\sigma}_{i+1}^y + \hat{\sigma}_i^z \hat{\sigma}_{i+1}^z). \quad (21)$$

We take $J = 1$ as the energy scale.

In Fig. 8, we show the error against χ for $L = 64$. The results show that the error decreases with the bond dimension χ for the DMRG and PT-DMRG. Amazingly, the error of the PT-DMRG decreases more rapidly than that of the standard DMRG. This shows a considerable improvement in the accuracy for any value of the bond dimension χ .

In Fig. 9, we show the fit of $\chi^{(DMRG)}$ against $\chi^{(PT)}$ for $L = 64$. Again, a linear relation is found between $\chi^{(PT)}$ and $\chi^{(DMRG)}$:

$$\chi^{(DMRG)} = 1.32\chi^{(PT)} + 0.23. \quad (22)$$

Especially, the slope is larger than that in the quantum Ising model, which implies a more significant improvement in efficiency when calculating the Heisenberg chain with a large bond dimension cutoff.

VI. THERMODYNAMIC LIMIT

In the following, we explore a second-order perturbation theory for the DMRG in the thermodynamic limit. In the previous section we showed that the error scaling of the PT-DMRG is linear in L^{-1} for moderate L . Now if L approaches infinity we have that the scaling law is $1/\sqrt{L}$.

We focus on the results in Fig. 5 first. If we extend the results to larger L , we can see a change in behavior for the large- L

limit; the error in the energy per site becomes exactly equal to that of the conventional DMRG. We can understand this by looking at how the PT-DMRG approaches the thermodynamic limit. The off-diagonal matrix elements of the effective Hamiltonian \mathcal{H}_{ij} for $|i - j| > 1$ decay exponentially quickly, so it really only needs a few of them. For the Ising model $\mathcal{H}_{i,i+2}$ is already $O(10^{-6})$, so this gives no improvement over the old style of calculating just the diagonal part and the overlap with the ground state. In the large- L limit, the effective Hamiltonian \mathcal{H}_{ij} can be well approximated by

$$\mathcal{H} = \begin{bmatrix} a & b & b & b & b & \dots \\ b & c & 0 & 0 & 0 & \dots \\ b & 0 & c & 0 & 0 & \dots \\ b & 0 & 0 & c & 0 & \dots \\ \vdots & \vdots & \vdots & \vdots & \vdots & \ddots \end{bmatrix}, \quad (23)$$

where the nonzero elements are $a = \langle \psi_0 | \hat{H} | \psi_0 \rangle$ at the top left (the energy of the original ground state), a series of L entries along the top row and left column which is $b = \langle \psi_i | \hat{H} | \psi_0 \rangle$ (assumed independent of i in the large L limit), and the diagonal entries $c = \langle \psi_i | H | \psi_i \rangle$ independent of i in the large- L limit. a and c are extensive in the system size, but c has a constant offset because of the local perturbation. So we can set

$$a = E_0 \times L, \quad c = E_0 \times L + q, \quad (24)$$

where q is the energy of the perturbation. It is possible to determine the perturbed ground-state energy as a function of L , which is

$$E = \left(E_0 \times L + \frac{q}{2} \right) - \Delta, \quad (25)$$

where

$$\Delta^2 = \frac{q^2}{4} + b^2 L. \quad (26)$$

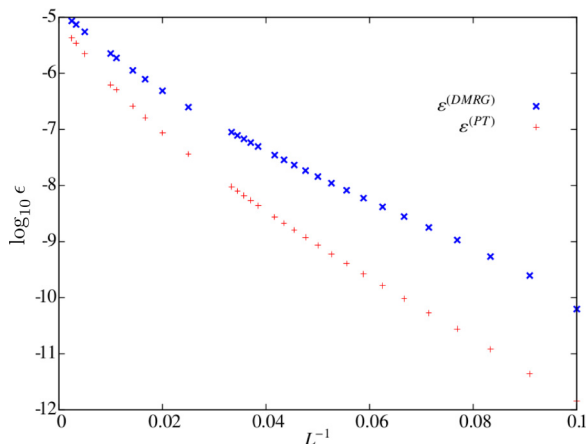


FIG. 10. Error ε of the 1D Ising model as a function of the length in the quantum phase transition $h = 1.0$, for $\chi = 8$. We show that the error of the PT-DMRG in the large- L limit does not give a systematic improvement in accuracy.

So now we can see the origin of the $1/\sqrt{L}$ behavior. For large L the energy per site scales as

$$\frac{E}{L} = E_0 - \frac{|b|}{\sqrt{L}} + O(1/L). \quad (27)$$

But in order to see the square root behavior $b^2 L \gg q^2/4$, which, for the Ising model, requires $L > 650$ (see Fig. 10). The plot in Fig. 10 is basically linearizing a square root in a region well away from the asymptotic large- L behavior.

VII. SUMMARY AND OUTLOOK

A simple and efficient numeric approach called the PT-DMRG is proposed to greatly improve the accuracy of the conventional DMRG. It gives a better approximation of the ground state of strongly correlated many-body systems by recovering the leading term of entanglement, which is discarded in the truncations of the DMRG. Using the MPS representation, we introduce a set of orthogonal bases to define the perturbed Hamiltonian, whose ground state possesses a better precision than the traditional DMRG. In other words, we use the Schmidt numbers that are beyond the dimension cutoff to define the perturbation terms. Using the second-order PT-DMRG, our numerical results obtained for the 1D quantum Ising model and Heisenberg model show a better accuracy reached by our PT-DMRG, where the precision of the DMRG is shown to be improved significantly [around $O(10)$ times]. As argued above, this is essentially caused by the fact that the PT-DMRG is able to capture more entanglement than the MPS from the standard DMRG.

Our PT-DMRG provides a fundamental scheme that can be directly used for the 2D DMRG algorithm. Such perturbation theory based on the MPS can be generalized to other MPSs or even tensor network algorithms, such as time-evolved block decimation. The generalization to higher-order perturbation theories is to be explored in the future.

Finally, the perturbation theories can provide a fundamental scheme for study of the power-law correlation. For example, in the Multi-scale Entanglement Renormalization Ansatz the isometries can be used to define perturbed terms. The kernel space of each original isometry provides the tangent space in a natural way. So the perturbation idea may be useful in any state ansatz that gives a renormalization flow.

ACKNOWLEDGMENTS

This work was supported by ERC ADG OSYRIS, EQuaM (FP7/2007-2013 Grant No. 323714), Spanish MINECO (Severo Ochoa Grant No. SEV-2015-0522), FOQUS (FIS2013-46768), FISICATEAMO (FIS2016-79508-P), Generalitat de Catalunya AGAUR Grant SGR 874, CERCA Program/Generalitat de Catalunya, Fundació Cellex, and EU FETPRO QUIC, Marie Curie fellowship SQSNP 622939 FP7-MC-IIIF.

APPENDIX: TWO-SITE DMRG: TECHNICAL DETAILS

In Sec. II we have briefly introduced the DMRG. Here we show the details of the DMRG algorithm. In order to obtain the ground state $|\psi_0\rangle$, one needs to find the MPS that minimizes

the following equation:

$$E = \frac{\langle \psi | \hat{H} | \psi \rangle}{\langle \psi | \psi \rangle}. \quad (\text{A1})$$

The most efficient way of doing this is to use a variational approach by minimizing E over the MPS family:

$$\min_{|\psi\rangle \in \text{MPS}} \{ \langle \psi | \hat{H} | \psi \rangle - \lambda \langle \psi | \psi \rangle \}. \quad (\text{A2})$$

To proceed with the minimization, we introduce two vectors:

$$|a_l\rangle_A = \sum_{\sigma_1 \dots \sigma_l} (A^{\sigma_1} \dots A^{\sigma_l})_{1, a_l} |\sigma_1 \dots \sigma_l\rangle, \quad (\text{A3})$$

$$|a_l\rangle_B = \sum_{\sigma_{l+1} \dots \sigma_L} (B^{\sigma_{l+1}} \dots B^{\sigma_L})_{a_l, 1} |\sigma_{l+1} \dots \sigma_L\rangle, \quad (\text{A4})$$

where the tensors A^{σ_i} and B^{σ_i} verified Eq. (6). Then state $|\psi\rangle$ can be written as

$$|\psi\rangle = \sum_{\sigma_l \sigma_{l+1} a_{l-1} a_{l+1}} D^{\sigma_l \sigma_{l+1}} |a_{l-1}\rangle_A |\sigma_l \sigma_{l+1}\rangle |a_{l+1}\rangle_B. \quad (\text{A5})$$

Then the minimization is written as

$$\begin{aligned} & \min_{|\psi\rangle \in \text{MPS}} \{ \langle \psi | \hat{H} | \psi \rangle - \lambda \langle \psi | \psi \rangle \} \\ & \rightarrow \min_D \{ D^\dagger \hat{H}_{\text{eff}} D - \lambda D^\dagger \hat{N} D \}. \end{aligned} \quad (\text{A6})$$

\hat{H}_{eff} and \hat{N} correspond to $\langle \psi | \hat{H} | \psi \rangle$ and $\langle \psi | \psi \rangle$ without D and D^\dagger , respectively. The term $-\lambda \langle \psi | \psi \rangle$ is introduced to make all eigenvalues negative, so that the MPS is generated to converge to the ground state. By considering D as a vector, the minimization becomes

$$\frac{\partial}{\partial D^\dagger} \{ D^\dagger \hat{H}_{\text{eff}} D - \lambda D^\dagger \hat{N} D \} = 0. \quad (\text{A7})$$

Let us first consider the overlap $\langle \psi | \psi \rangle$. As shown in Fig. 11, we use Eq. (A5),

$$\begin{aligned} \langle \psi | \psi \rangle &= \sum_{\sigma_l \sigma_{l+1}} \sum_{a_{l-1} a'_{l-1}} \sum_{a_{l+1} a'_{l+1}} T^A_{a_{l-1} a'_{l-1}} D^{\sigma_l \sigma_{l+1}} \\ &\quad \cdot D^{\sigma_l \sigma_{l+1}} \dagger T^B_{a_{l+1} a'_{l+1}}, \end{aligned} \quad (\text{A8})$$

where $T^A_{a_{l-1}, a'_{l-1}}$ and $T^B_{a_{l+1}, a'_{l+1}}$ are

$$\begin{aligned} T^A_{a_{l-1}, a'_{l-1}} &= \sum_{\sigma_1 \dots \sigma_{l-1}} (A^{\sigma_1 \dagger} \dots A^{\sigma_{l-1} \dagger} A^{\sigma_1} \dots A^{\sigma_{l-1}})_{a_{l-1}, a'_{l-1}}, \quad (\text{A9}) \\ T^B_{a_{l+1}, a'_{l+1}} &= \sum_{\sigma_{l+2} \dots \sigma_L} (B^{\sigma_{l+2}} \dots B^{\sigma_L} B^{\sigma_{l+2} \dagger} \dots B^{\sigma_L \dagger})_{a_{l+1}, a'_{l+1}}. \end{aligned} \quad (\text{A10})$$

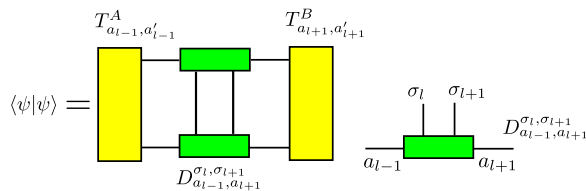


FIG. 11. Graphical representation of $\langle \psi | \psi \rangle$ through the two-rank tensors T^A and T^B .

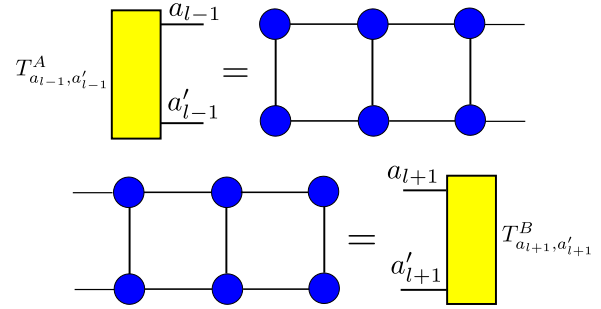


FIG. 12. Graphical representation of the matrices T^A and T^B that contain the contraction.

The tensor \hat{T}^A (\hat{T}^B) contains all the contraction of tensors of the MPS from site 1 to site $l-1$ (site $l+2$ to site L) (see Fig. 12). If the bases from site 1 to site $l-1$ are left-orthogonal and the basis from site $l+1$ to site N are right-orthogonal, we simply have

$$T^A_{a_{l-1}, a'_{l-1}} = \delta_{a_{l-1}, a'_{l-1}}, \quad T^B_{a_{l+1}, a'_{l+1}} = \delta_{a_{l+1}, a'_{l+1}}. \quad (\text{A11})$$

We show below that such left- and right-orthogonal conditions are automatically fulfilled in the DMRG.

$\langle \psi | \hat{H} | \psi \rangle$ is described in the tensor network in Fig. 13 that contains the contraction between two MPSs and the MPO. Therefore, one has

$$\begin{aligned} \langle \psi | \hat{H} | \psi \rangle &= \sum_{\sigma_l \sigma_{l+1} a_{l-1} a_{l+1}} \sum_{\sigma'_l \sigma'_{l+1} a'_{l-1} a'_{l+1}} D^{\sigma_l \sigma_{l+1}} \dagger D^{\sigma'_l \sigma'_{l+1}} \\ &\quad \cdot \langle a_{l-1} \sigma_l \sigma_{l+1} a_{l+1} | \hat{H} | a'_{l-1} \sigma'_l \sigma'_{l+1} a'_{l+1} \rangle. \end{aligned} \quad (\text{A12})$$

Let us now look at the matrix elements $\langle a_{l-1} \sigma_l \sigma_{l+1} a_{l+1} | \hat{H} | a'_{l-1} \sigma'_l \sigma'_{l+1} a'_{l+1} \rangle$ using the MPO representation of Hamiltonian \hat{H} :

$$\begin{aligned} & \langle a_{l-1} \sigma_l \sigma_{l+1} a_{l+1} | \hat{H} | a'_{l-1} \sigma'_l \sigma'_{l+1} a'_{l+1} \rangle \\ &= \sum_{\sigma \sigma'} W^{\sigma \sigma'} \dots W^{\sigma_L \sigma'_L} \cdot \langle a_{l-1} \sigma_l \sigma_{l+1} a_{l+1} | \sigma_1 \dots \sigma_L \rangle \\ &\quad \times \langle \sigma'_1 \dots \sigma'_L | a'_{l-1} \sigma'_l \sigma'_{l+1} a'_{l+1} \rangle. \end{aligned} \quad (\text{A13})$$

Using Eqs. (A3) and (A4), we can evaluate the scalar product in the previous equation:

$$\begin{aligned} & \langle a_{l-1} \sigma_l \sigma_{l+1} a_{l+1} | \sigma'_1 \dots \sigma'_L \rangle \\ &= (A^{\sigma_1 \dagger} \dots A^{\sigma_{l-1} \dagger})_{1, a_{l-1}} \cdot (B^{\sigma_{l+2} \dagger} \dots B^{\sigma_L \dagger})_{a_{l+1}, 1}, \end{aligned} \quad (\text{A14})$$

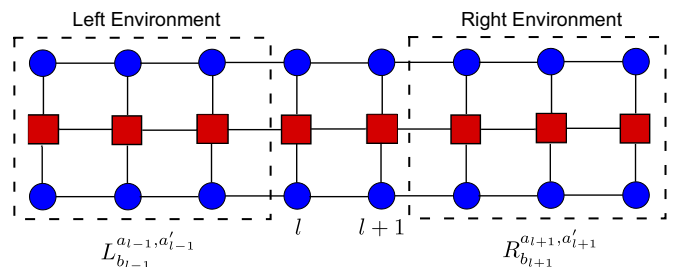


FIG. 13. Tensor network represented the quantity $\langle \psi | \hat{H} | \psi \rangle$.

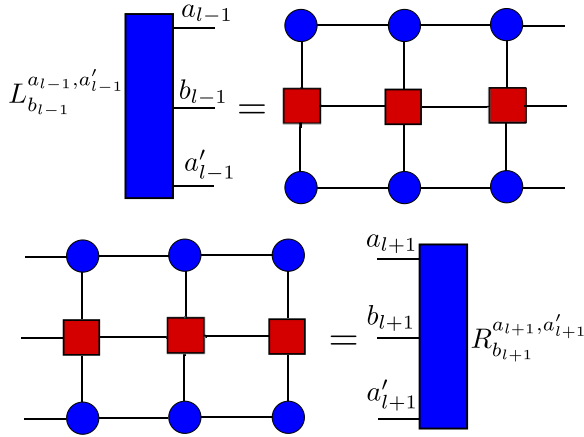


FIG. 14. Graphical representation of the environment left L and right R , where L contains the contracted left part, while R contains the contracted right part of the network.

$$\begin{aligned} & \langle \sigma'_1 \cdots \sigma'_L | \alpha' \sigma'_1 \sigma'_{l+1} \beta' \rangle \\ & = (A^{\sigma'_1} \cdots A^{\sigma'_{l-1}})_{1, a'_{l-1}} \cdot (B^{\sigma'_{l+2}} \cdots B^{\sigma'_L})_{a'_{l+1}, 1}. \end{aligned} \quad (\text{A15})$$

Define the tensors L and R that contain the contracted left and right halves as (see Fig. 14)

$$\begin{aligned} L_{b_{l-1}}^{a_{l-1}, a'_{l-1}} & = \left\{ \sum_{\sigma_1 \sigma'_1} A_{1, a_1}^{\sigma_1} \dagger W_{1, b_1}^{\sigma_1 \sigma'_1} A_{1, a'_1}^{\sigma'_1} \right\} \\ & \cdots \left\{ \sum_{\sigma_{l-1} \sigma'_{l-1}} A_{a_{l-2}, a_{l-1}}^{\sigma_{l-1}} \dagger W_{b_{l-2}, b_{l-1}}^{\sigma_{l-1} \sigma'_{l-1}} A_{a'_{l-2}, a'_{l-1}}^{\sigma'_{l-1}} \right\}, \quad (\text{A16}) \\ R_{b_{l+1}}^{a_{l+1}, a'_{l+1}} & = \left\{ \sum_{\sigma_{l+2} \sigma'_{l+2}} B_{a_{l+1}, a_{l+2}}^{\sigma_{l+2}} \dagger W_{b_{l+1}, b_{l+2}}^{\sigma_{l+2} \sigma'_{l+2}} B_{a'_{l+1}, a'_{l+2}}^{\sigma'_{l+2}} \right\} \\ & \cdots \left\{ \sum_{\sigma_L \sigma'_L} B_{a_{L-1}, 1}^{\sigma_L} \dagger W_{b_{L-1}, 1}^{\sigma_L \sigma'_L} B_{a'_{L-1}, 1}^{\sigma'_L} \right\}. \quad (\text{A17}) \end{aligned}$$

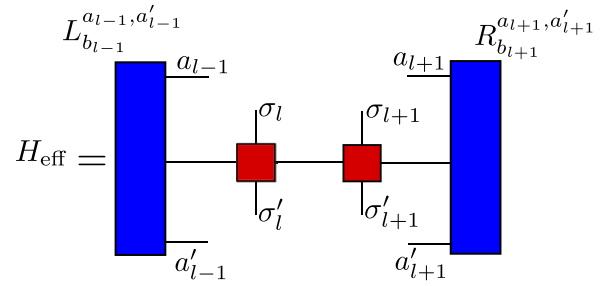


FIG. 15. Graphical representation of the effective Hamiltonian H_{eff} defined in Eq. (A21).

Through Eqs. (A16) and (A17), we obtain

$$\begin{aligned} & \langle a_{l-1} \sigma_l \sigma_{l+1} a_{l+1} | \hat{H} | a'_{l-1} \sigma'_l \sigma'_{l+1} a'_{l+1} \rangle \\ & = \sum_{b_{l-1} b_{l+1}} L_{b_{l-1}}^{a_{l-1}, a'_{l-1}} W_{b_{l-1} b_l}^{\sigma_l \sigma'_l} W_{b_l b_{l+1}}^{\sigma_{l+1} \sigma'_{l+1}} R_{b_{l+1}}^{a_{l+1}, a'_{l+1}}. \end{aligned} \quad (\text{A18})$$

Now we can immediately write $\langle \psi | \hat{H} | \psi \rangle$ as

$$\begin{aligned} \langle \psi | \hat{H} | \psi \rangle & = \sum_{a_{l-1} a'_{l-1}} \sum_{a_{l+1} a'_{l+1}} \sum_{\sigma_l \sigma'_l} \sum_{\sigma_{l+1} \sigma'_{l+1}} D_{a_{l-1} a_{l+1}}^{\sigma_l \sigma_{l+1}} \dagger D_{a'_{l-1} a'_{l+1}}^{\sigma'_l \sigma'_{l+1}} \\ & \cdot L_{b_{l-1}}^{a_{l-1}, a'_{l-1}} W_{b_{l-1} b_l}^{\sigma_l \sigma'_l} W_{b_l b_{l+1}}^{\sigma_{l+1} \sigma'_{l+1}} R_{b_{l+1}}^{a_{l+1}, a'_{l+1}} \end{aligned} \quad (\text{A19})$$

and rewrite Eq. (A7) as

$$\begin{aligned} & \left(\sum_{a'_{l-1} a'_{l+1}} \sum_{\sigma_l \sigma'_l} \sum_{\sigma_{l+1} \sigma'_{l+1}} L_{b_{l-1}}^{a_{l-1}, a'_{l-1}} W_{b_{l-1} b_l}^{\sigma_l \sigma'_l} W_{b_l b_{l+1}}^{\sigma_{l+1} \sigma'_{l+1}} R_{b_{l+1}}^{a_{l+1}, a'_{l+1}} \right. \\ & \left. - \lambda \sum_{a_{l-1} a'_{l-1}} T_{a_{l-1}, a'_{l-1}}^A T_{a_{l+1}, a'_{l+1}}^B \right) D_{a_{l-1} a'_{l+1}}^{\sigma_l \sigma_{l+1}} = 0. \end{aligned} \quad (\text{A20})$$

The matrices H_{eff} (see Fig. 15) and N simply are

$$H_{\text{eff}} = \sum_{b_{l-1} b_{l+1}} L_{b_{l-1}}^{a_{l-1}, a'_{l-1}} W_{b_{l-1} b_l}^{\sigma_l \sigma'_l} W_{b_l b_{l+1}}^{\sigma_{l+1} \sigma'_{l+1}} R_{b_{l+1}}^{a_{l+1}, a'_{l+1}}, \quad (\text{A21})$$

$$N = T_{a_{l-1}, a'_{l-1}}^A T_{a_{l+1}, a'_{l+1}}^B. \quad (\text{A22})$$

Using the expressions above, we find the minimization defined in Eq. (9).

- [1] S. Sachdev, *Quantum Phase Transitions*, 2nd ed. (Cambridge University Press, Cambridge, UK, 2011).
- [2] C. Lacroix, P. Mendels, and F. Mila, *Introduction to Frustrated Magnetism* (Springer, Heidelberg, 2011).
- [3] M. Lewenstein, A. Sanpera, and V. Ahufinger, *Ultracold Atoms in Optical Lattices: Simulating Quantum Many-Body Systems* (Oxford University Press, New York, 2012).
- [4] C. Castelnovo, R. Moessner, and S. Sondhi, Spin ice, fractionalization, and topological order, *Ann. Rev. Condens. Matter Phys.* **3**, 35 (2012).
- [5] P. W. Anderson, The resonating valence bond state in La_2CuO_4 and superconductivity, *Science* **235**, 1196 (1987).
- [6] P. A. Lee, N. Nagaosa, and X. G. Wen, Doping a Mott insulator: Physics of high-temperature superconductivity, *Rev. Mod. Phys.* **78**, 17 (2006).
- [7] J. M. Kosterlitz and J. Thouless, Long range order and metastability in two dimensional solids and superfluids (application of dislocation theory), *Solid State Phys.* **5**, L124 (1972).
- [8] B. A. Bernevig and T. L. Hughes, *Topological Insulators and Topological Superconductors* (Princeton University Press, Princeton, NJ, 2013).
- [9] L. Balents, Spin liquids in frustrated magnets, *Nature* **464**, 199 (2010).
- [10] A. Banerjee, C. A. Bridges, J.-Q. Yan, A. A. Aczel, L. Li, M. B. Stone, G. E. Granroth, M. D. Lumsden, Y. Yiu, J. Knolle, S. Bhattacharjee, D. L. Kovrizhin, R. Moessner, D. A. Tennant, D. G. Mandrus, and S. E. Nagler, Proximate Kitaev quantum spin liquid behavior in a honeycomb magnet, *Nat. Mater.* **15**, 733 (2016).

- [11] H. Bethe, On the theory of metals. I. Eigenvalues and eigenfunctions of the linear atom chain, *Z. Phys. A* **71**, 205 (1931).
- [12] E. H. Lieb and F. Y. Wu, Absence of Mott Transition in an Exact Solution of the Short-Range, One-Band Model in One Dimension, *Phys. Rev. Lett.* **20**, 1445 (1968).
- [13] F. H. L. Essler, H. Frahm, F. Göhmann, A. Klümper, and V. E. Körepin, *The One-Dimensional Hubbard Model* (Cambridge University Press, Cambridge, UK, 2005).
- [14] A. W. Sandvik, Computational studies of quantum spin systems, *AIP Conf. Proc.* **1297**, 135 (2010).
- [15] M. Troyer and U. J. Wiese, Computational Complexity and Fundamental Limitations to Fermionic Quantum Monte Carlo Simulations, *Phys. Rev. Lett.* **94**, 170201 (2005).
- [16] U. Schollwöck, The density-matrix renormalization group in the age of matrix product states, *Ann. Phys.* **326**, 96 (2011).
- [17] R. Orus, A practical introduction to tensor networks: Matrix product states and projected entangled pair states, *Ann. Phys.* **349**, 117 (2014).
- [18] J. Eisert, M. Cramer, and M. B. Plenio, Area laws for the entanglement entropy, *Rev. Mod. Phys.* **82**, 277 (2010).
- [19] G. Vidal, J. I. Latorre, E. Rico, and A. Kitaev, Entanglement in Quantum Critical Phenomena, *Phys. Rev. Lett.* **90**, 227902 (2003).
- [20] J. I. Latorre, E. Rico, and G. Vidal, Ground state entanglement in quantum spin chains, *Quant. Inf. Comput.* **4**, 48 (2004).
- [21] I. Peschel, M. Kaulke, and O. Legeza, Density-matrix spectra for integrable models, *Ann. Phys. (Leipzig)* **8**, 153 (1999).
- [22] J. D. Bekenstein, Black holes and entropy, *Phys. Rev. D* **7**, 2333 (1973).
- [23] M. Srednicki, Entropy and Area, *Phys. Rev. Lett.* **71**, 666 (1993).
- [24] M. B. Plenio, J. Eisert, J. Dreissig, and M. Cramer, Entropy, Entanglement, and Area: Analytical Results for Harmonic Lattice Systems, *Phys. Rev. Lett.* **94**, 060503 (2005).
- [25] P. Calabrese and J. Cardy, Entanglement entropy and quantum field theory, *J. Stat. Mech.* (2004) P06002.
- [26] U. Schollwöck, The density-matrix renormalization group, *Rev. Mod. Phys.* **77**, 259 (2005).
- [27] K. A. Hallberg, New trends in density matrix renormalization, *Adv. Phys.* **55**, 477 (2006).
- [28] S. R. White, Density Matrix Formulation for Quantum Renormalization Groups, *Phys. Rev. Lett.* **69**, 2863 (1992).
- [29] S. R. White, Density-matrix algorithms for quantum renormalization groups, *Phys. Rev. B* **48**, 10345 (1993).
- [30] K. G. Wilson, The renormalization group: Critical phenomena and the Kondo problem, *Rev. Mod. Phys.* **47**, 773 (1975).
- [31] S. Östlund and S. Rommer, Thermodynamic Limit of Density Matrix Renormalization, *Phys. Rev. Lett.* **75**, 3537 (1995).
- [32] F. Verstraete, D. Porras, and J. I. Cirac, Density Matrix Renormalization Group and Periodic Boundary Conditions: A q Information Perspective, *Phys. Rev. Lett.* **93**, 227205 (2004).
- [33] R. J. Baxter, *Exactly Solved Models in Statistical Mechanics* (Academic Press, London, 1982).
- [34] J. Hubbard, Electron correlations in narrow energy bands, *Proc. Roy. Soc.* **276**, 238 (1963).
- [35] J. Hubbard, Electron correlations in narrow energy bands. III. An improved solution, *Proc. Roy. Soc.* **281**, 401 (1964).
- [36] J. Kanamori, Electron correlation and ferromagnetism of transition metals, *Prog. Theor. Phys.* **30**, 275 (1963).
- [37] M. C. Gutzwiller, Effect of Correlation on the Ferromagnetism of Transition Metals, *Phys. Rev. Lett.* **10**, 159 (1963).
- [38] M. Lewenstein, A. Sanpera, V. Ahufinger, B. Damski, A. Sen De, and U. Sen, Ultracold atomic gases in optical lattices: Mimicking condensed matter physics and beyond, *Adv. Phys.* **56**, 243 (2007).
- [39] S. R. White and D. A. Huse, Numerical renormalization-group study of low-lying eigenstates of the antiferromagnetic $S = 1$ Heisenberg chain, *Phys. Rev. B* **48**, 3844 (1993).
- [40] E. S. Sørensen and I. Affleck, $S(k)$ for Haldane-gap antiferromagnets: Large-scale numerical results versus field theory and experiment, *Phys. Rev. B* **49**, 13235 (1994).
- [41] E. S. Sørensen and I. Affleck, Equal-time correlations in Haldane-gap antiferromagnets, *Phys. Rev. B* **49**, 15771 (1994).
- [42] J. Spalek, t-J model then and now: A personal perspective from the pioneering times, *Acta Phys. Pol. A* **111**, 409 (2007).
- [43] U. Schollwöck and T. Jolicoeur, Haldane gap and hidden order in the $S = 2$ antiferromagnetic quantum spin chain, *Europhys. Lett.* **30**, 493 (1995).
- [44] S. W. Tsai and J. B. Marston, Study of critical behavior of the supersymmetric spin chain that models plateau transitions in the integer quantum Hall effect, *Ann. Phys. (Leipzig)* **8**, 261 (1999).
- [45] E. M. Stoudenmire and S. R. White, Studying two dimensional systems with the density matrix renormalization group, *Annu. Rev. Condens. Matter Phys.* **3**, 111 (2012).
- [46] A. Kitaev and J. Preskill, Topological Entanglement Entropy, *Phys. Rev. Lett.* **96**, 110404 (2006).
- [47] S. Yan, D. A. Huse, and S. R. White, Spin liquid ground state of the $S = 1/2$ Kagome Heisenberg model, *Science* **332**, 1173 (2011).
- [48] M. Q. Weng, D. N. Sheng, Z. Y. Weng, and R. J. Bursill, Spin-liquid phase in an anisotropic triangular-lattice Heisenberg model: Exact diagonalization and density-matrix renormalization group calculations, *Phys. Rev. B* **74**, 012407 (2006).
- [49] H. C. Jiang, Z. Y. Weng, and D. N. Sheng, Density Matrix Renormalization Group Numerical Study of the Kagome Antiferromagnet, *Phys. Rev. Lett.* **101**, 117203 (2008).
- [50] L. Capriotti, D. J. Scalapino, and S. R. White, Spin-liquid versus dimerized ground states in a frustrated Heisenberg antiferromagnet, *Phys. Rev. Lett.* **93**, 177004 (2004).
- [51] S. S. Gong, W. Zhu, and D. N. Sheng, Emergent chiral spin liquid: Fractional quantum Hall effect in a kagome Heisenberg model, *Sci. Rep.* **4**, 6317 (2014); Y. C. He, D. N. Sheng, and Y. Chen, Chiral Spin Liquid in a Frustrated Anisotropic Kagome Heisenberg Model, *Phys. Rev. Lett.* **112**, 137202 (2014).
- [52] S. S. Gong, W. Zhu, L. Balents, and D. N. Sheng, Global phase diagram of competing ordered and quantum spin-liquid phases on the kagome lattice, *Phys. Rev. B* **91**, 075112 (2015).
- [53] H. C. Jiang, F. Kruger, J. E. Moore, D. N. Sheng, J. Zaanen, and Z. Y. Weng, Phase diagram of the frustrated spatially-anisotropic $S = 1$ antiferromagnet on a square lattice, *Phys. Rev. B* **79**, 174409 (2009).
- [54] D. N. Sheng, O. I. Motrunich, and M. P. A. Fisher, Spin Bose-metal phase in a spin-1/2 model with ring exchange on a two-leg triangular strip, *Phys. Rev. B* **79**, 205112 (2009).
- [55] M. S. Block, D. N. Sheng, O. I. Motrunich, and M. P. A. Fisher, Spin Bose-Metal and Valence Bond Solid Phases in a Spin-1/2 Model with Ring Exchanges on a Four-Leg Triangular Ladder, *Phys. Rev. Lett.* **106**, 157202 (2011).
- [56] S. R. White, R. M. Noack, and D. J. Scalapino, Resonating Valence Bond Theory of Coupled Heisenberg Chains, *Phys. Rev. Lett.* **73**, 886 (1994).

- [57] K. A. Hallberg, Density-matrix algorithm for the calculation of dynamical properties of low-dimensional systems, *Phys. Rev. B* **52**, R9827(R) (1995).
- [58] S. Ramasesha, S. K. Pati, H. R. Krishnamurthy, Z. Shuai, and J. L. Brédas, *Synth. Met.* **85**, 1019 (1997).
- [59] T. D. Kuhner and S. R. White, Dynamical correlation functions using the density matrix renormalization group, *Phys. Rev. B* **60**, 335 (1999).
- [60] E. Jeckelmann, Dynamical density-matrix renormalization-group method, *Phys. Rev. B* **66**, 045114 (2002).
- [61] T. Nishino, Density matrix renormalization group method for 2D classical models, *J. Phys. Soc. Jpn.* **64**, 3598 (1995).
- [62] X. Q. Wang and T. Xiang, Transfer-matrix density-matrix renormalization-group theory for thermodynamics of one-dimensional quantum systems, *Phys. Rev. B* **56**, 5061 (1997).
- [63] N. Shibata, Thermodynamics of the anisotropic Heisenberg chain calculated by the density matrix renormalization group method, *J. Phys. Soc. Jpn.* **66**, 2221 (1997).
- [64] Y. Hieida, Application of the density matrix renormalization group method to a non-equilibrium problem, *J. Phys. Soc. Jpn.* **67**, 369 (1998).
- [65] E. Carlon, M. Henkel, and U. Schollwöck, Density matrix renormalization group and reaction-diffusion processes, *Eur. J. Phys. B* **12**, 99 (1999).
- [66] M. Henkel and U. Schollwöck, Universal finite-size scaling amplitudes in anisotropic scaling, *J. Phys. A* **34**, 3333 (2001).
- [67] J. Haegeman, T. J. Osborne, and F. Verstraete, Post-matrix product state methods: To tangent space and beyond, *Phys. Rev. B* **88**, 075133 (2013).
- [68] M. B. Lepetit and G. M. Pastor, Density-matrix renormalization using three classes of block states, *Phys. Rev. B* **58**, 12691 (1998).
- [69] C. Hubig, I. P. McCulloch, U. Schollwöck, and F. A. Wolf, A strictly single-site DMRG algorithm with subspace expansion, *Phys. Rev. B* **91**, 155115 (2015).
- [70] J. Dukelsky, M. A. Martin-Delgado, T. Nishino, and G. Sierra, Equivalence of the variational matrix product method and the density matrix renormalization group applied to spin chains, *Europhys. Lett.* **43**, 457 (1998).
- [71] G. M. Crosswhite, A. C. Doherty, and G. Vidal, Applying matrix product operators to model systems with long-range interactions, *Phys. Rev. B* **78**, 035116 (2008).
- [72] V. Nebendahl and W. Dür, Improved numerical methods for infinite spin chains with long-range interactions, *Phys. Rev. B* **87**, 075413 (2013).
- [73] I. P. McCulloch, Infinite size density matrix renormalization group, [arXiv:0804.2509](https://arxiv.org/abs/0804.2509).